Experimental Study on Semi-Active Control of Bridges with Use of Magnetorheological Damper

Anat Ruangrassamee*, Kazuhiko Kawashima**

* M. of Eng., Graduate Student, Dept. of Civil Eng., Tokyo Institute of Technology, 2-12-1, O-okayama, Meguro-ku, Tokyo 152-8552
** Dr. of Eng., Professor, Dept. of Civil Eng., Tokyo Institute of Technology, 2-12-1, O-okayama, Meguro-ku, Tokyo 152-8552

This study was conducted to investigate the application of a magnetorheological (MR) damper in the semi-active control of bridge response. A series of cyclic loading tests was carried out on a MR damper under various loading frequencies, loading amplitudes, and current levels. The damping force of the MR damper was idealized by the model composed of the friction and viscous elements in parallel. Two algorithms to change the damping force according to displacement or velocity were investigated. It is found that the commanded damping force can be realized by the MR damper. However, discrepancy of damping force is observed, especially when the rate of change of the damping force is high. The shaking table test was conducted on a model bridge with the MR damper to investigate the effectiveness of the control algorithms. Subsequently, the correlative study was performed by comparing the dynamic response of the bridge model obtained from the shaking table test with that obtained from analysis.

Key Words: magnetorheological damper, variable damper, semi-active control, control algorithm

1. Introduction

Under strong ground excitation, bridge piers may experience nonlinearity and bridge decks unseat from piers or abutments. Highway bridges are conventionally designed to behave passively during earthquakes. The seismic performance of the bridges is assured for some particular target ground motions. However, earthquake motion is stochastic in its nature. There arises the need to make structural properties more adaptive to responses caused by the unpredictable earthquake motion. To deal with the problem, many researchers have attempted to apply the active and semi-active control systems in the civil engineering structures.

Active control systems have been proved to reduce structural response. However, the response reduction is obtained at the expense of substantial power supply. In addition, the stability requirement of the active control systems limits its applicability. Semi-active control systems come in-between to bridge the gap. Semi-active control systems offer the reliability of passive devices, yet provide the adaptability of active control systems. Because the semi-active control systems are inherently stable and require much less amount of power supply, it is promising to apply the semi-active control systems to civil engineering structures[1].

Semi-active devices have been developed in the recent past decade. Semi-active viscous dampers provide adaptable damping force by adjusting the size of the orifice through which viscous fluid flows when a piston moves in a hydraulic cylinder[2]. Recently, magetorheological (MR) dampers gain interest from researchers[3, 4]. MR fluid is not sensitive to impurities commonly encountered during manufacturing and usage. MR fluid can be controlled with low power supply (less than 50W).

The study was conducted to investigate the application of a magnetorheological (MR) damper in the semi-active control of bridge response. A series of cyclic loading test was carried out on a MR damper under various loading frequencies, loading amplitudes, and current levels. Two algorithms to vary the damping force according to relative displacement or relative velocity were investigated. The shaking table test was conducted on a bridge model with the MR damper. Subsequently, the correlative study was performed by comparing the dynamic response of the bridge model with that obtained from analysis.

2. Cyclic Loading Test of MR Damper

A RD-1005-5-2 MR damper developed by Lord Corporation is used in this study. The damper is 208 mm long in its extended position and 155 mm long in its compressed position. So, the stroke of the damper is about +/- 25 mm. The cylinder is 41 mm in diameter. The damper operates at the current of 0-2 A. The current is supplied to the damper by a Lord RD-3002 current driver. The current driver outputs a 0-2 A output current proportional to a 0-5 V commanded input voltage.

In order to apply the MR damper as a semi-active control device, it is necessary to identify the damping properties of the MR damper. A series of cyclic loading tests was conducted for various loading conditions. Fig. 1 shows the

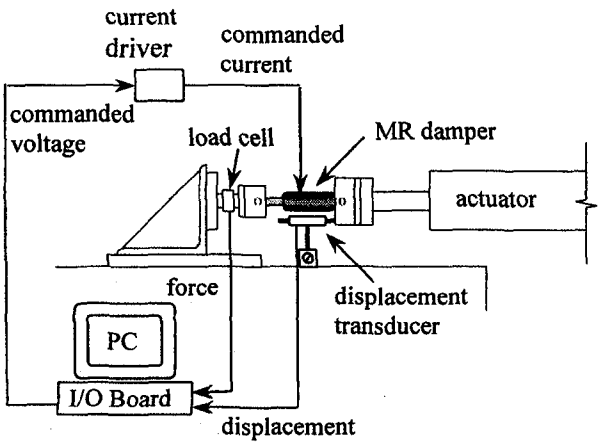

Fig. 1 Test setup of the cyclic loading test

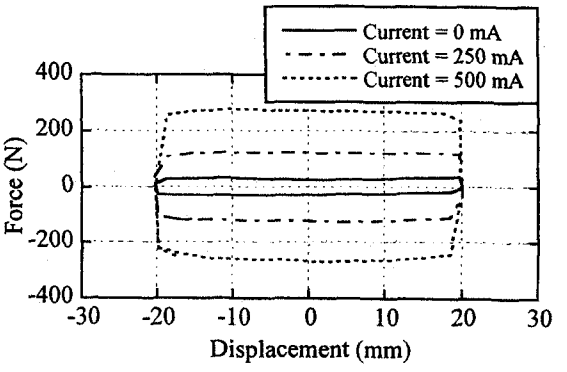

Fig. 2 Force-displacement relationship for the low-frequency loading

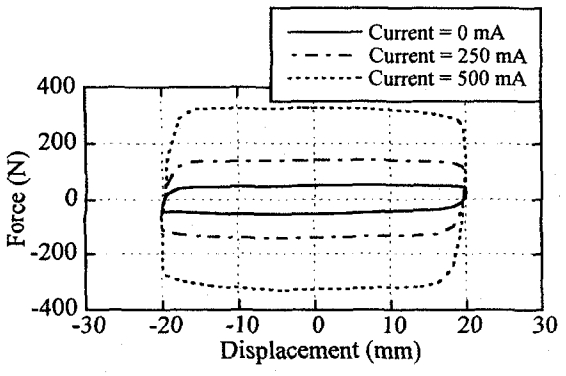

(a) force-displacement relationship

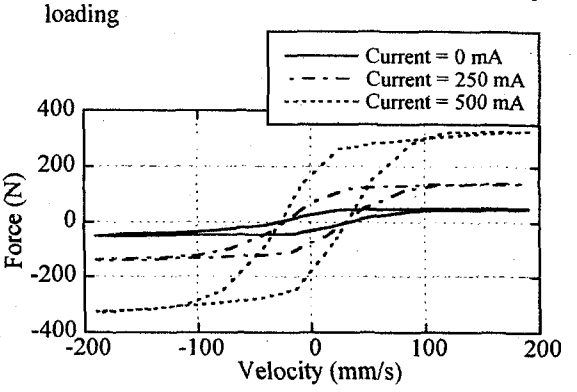

(b) force-velocity relationship

Fig.3 Response of the MR damper subjected to 1.5 Hz sinusoidal excitation with the amplitude of 20 mm

test setup of the cyclic loading test. The damping force was measured by a load cell. The load cell was connected between the reaction frame and the damper. The displacement was measured by a displacement transducer. The current to the damper was controlled by a microcomputer. The commanded voltage was generated by an I/O board which was installed in the computer. Then, the current driver supplied a current proportional to the commanded voltage. A hydraulic actuator with displacement control was used to load the damper.

The damper was loaded under a sinusoidal signal with a fixed frequency and amplitude, while the current to the damper was hold constant. The response of the damper was investigated for a wide range of loading frequencies, loading amplitudes, and current levels. The loading frequencies were 0.5, 1.0, 1.5, 2.0, and 2.5 Hz. The loading amplitudes were 5, 10, 15, and 20 mm. The current level was varied as 0, 50, 100, 150, 200, 250, 500, and 750 mA. In addition, a low-frequency loading test was conducted for those current levels under the loading frequency of 0.05 Hz and the amplitude of 20 mm.

Fig. 2 shows the force-displacement relationships of the low-frequency loading test for the current levels of 0, 250, and 500 mA. The force-displacement relationships are close to the rectangular shape which is typical for a friction damper. The damping force at maximum velocity is 27, 121, and 274 N for the current levels of 0, 250, and 500 mA, respectively.

Fig. 3 shows the response of the MR damper subjected to a 1.5 Hz sinusoidal excitation with the amplitude of 20 mm under the current levels of 0, 250, and 500 mA. It is seen that the damping force increases as the current to the damper increases. From Fig. 3 (a), the force-displacement relationship of the MR damper is close to that of a friction damper. Focusing on the positive-velocity region of the force-velocity relationship in Fig. 3 (b), the damping force varies linearly with velocity in the upper branch of the curve. However, the damping force decreases rapidly when the velocity is close to zero. The change of the damping force at velocity close to zero is not so sudden as a friction damper because of the blow-by of fluid between the piston and the cylinder. This can be obviously seen at the maximum displacement in the force-displacement relationship. When the direction of loading is reversed, small movement is required before the damper reaches a certain level of force, causing smooth change of force.

Fig. 4 illustrates the comparison of the force-displacement relationships for various loading frequencies, loading amplitudes, and current levels. It is seen that the shape of force-displacement relationship is not significantly affected by the loading conditions. For a fixed current level, the damping force increases slightly as the loading frequency or loading amplitude increases.

3. Model of MR Damper

To control the damping force of the MR damper, the model of the MR damper is essential. In this study, the MR damper is modeled by the friction and viscous elements in parallel as illustrated in Fig. 5. The damping force is expressed as

$$f_d = f + cv \tag{1}$$

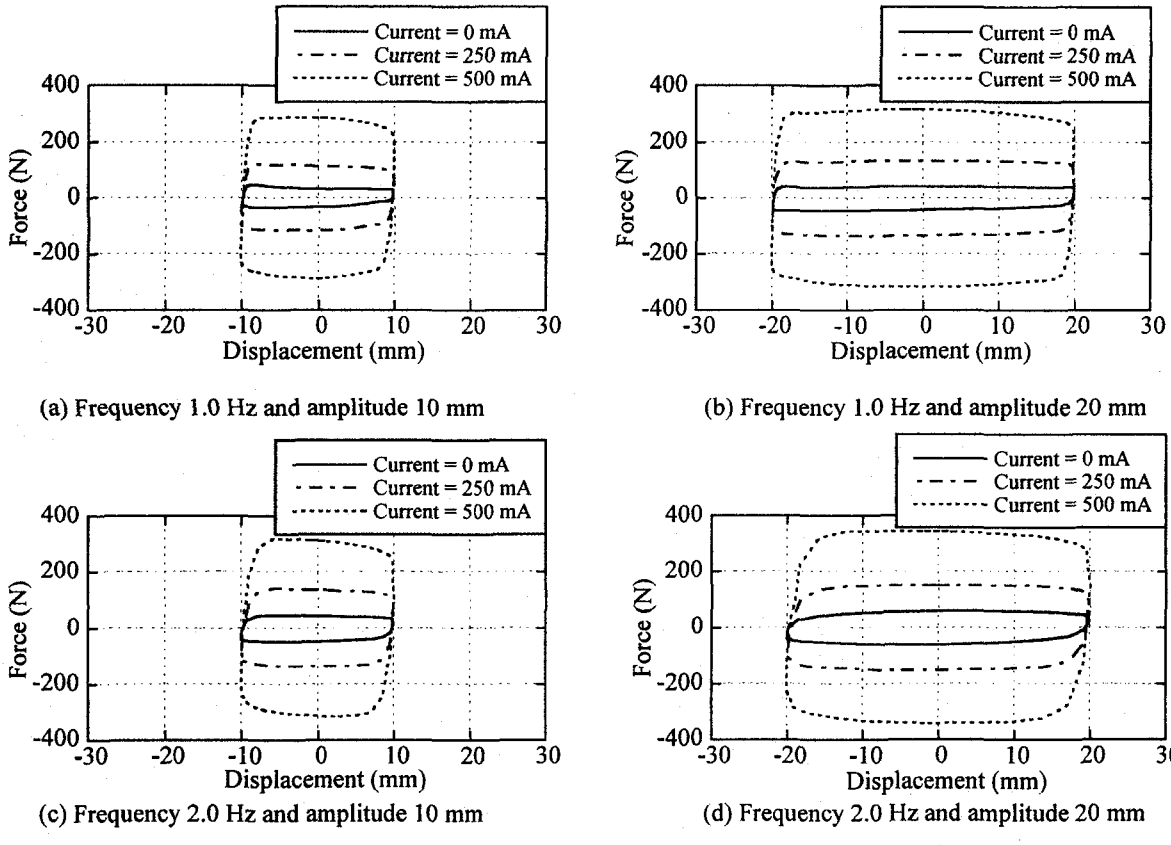

(a) Frequency 1.0 Hz and amplitude 10 mm

(b) Frequency 1.0 Hz and amplitude 20 mm

(c) Frequency 2.0 Hz and amplitude 10 mm

(d) Frequency 2.0 Hz and amplitude 20 mm

Fig.4 Response of the MR damper subjected to various loading conditions

where f_d is damping force, f is friction force, c is a damping coefficient, and v is velocity.

From the experimental results, maximum loading velocity and damping force at the maximum velocity are determined for various current levels as shown in Fig. 6. It is found that for a particular current, the damping force varies quite linearly with the velocity. As the current increases, the damping force at certain velocity increases. The damping force for each current level is modeled according to Eq. (1) by the regression analysis of the experimental results. Consequently, the dependencies of f and c on the current are expressed as

$$f=\begin{cases} 22.6+0.267\times current & ;\ current<200mA \\ -53.4+0.647\times current & ;\ current>200mA \end{cases} \quad (2)$$

$$c=0.113+0.000327\times current \quad (3)$$

where f is in N, c is in Ns/mm, and *current* is in mA. Fig. 7 shows the comparison of the parameters f and c determined from the regression analysis of the experimental results and those determined from Eqs. (2) and (3). The damping force predicted by Eqs. (1)- (3) is illustrated in Fig. 8. Comparing Fig. 6 to Fig. 8, it is seen that the damping force can be predicted by Eqs. (1)-(3) with good accuracy.

4. MR Damper under Fluctuating Current

The model of the MR damper was developed based on the cyclic loading test under constant current. In actual control application, the damper is subjected to fluctuating current depending on the measured structural response. So, the characteristic of the damper under fluctuating current needs to be investigated.

When the current is suddenly applied to the damper, certain time is required for MR fluid to reach its rheological equilibrium. Referring to Fig. 9, when a square current with a certain time interval is supplied to the damper, the damping force increases and then becomes constant. The rise time t_r is defined as the duration from the time of applying the current to the time that the damping force becomes constant. And when the current is terminated, the damping force decreases and then becomes constant. The fall time t_f is defined as the duration from the time of terminating the current to the time that the damping force becomes constant.

To determine the rise time and the fall time, a cyclic loading test was conducted under square currents with various time intervals and current levels. Fig. 10 shows time histories of damping force measured from the experiment and that predicted from Eqs. (1)-(3) for a 0.5 Hz sinusoidal excitation with an amplitude of 20 mm. It is seen that for the time interval of 40 ms, the measured damping force is smaller than the predicted damping force. But when the time interval of 140 ms is provided, the maximum values of the measured and predicted damping force are very close. The measured and predicted values of the increased damping force after applying current is represented by a force ratio R_f defined as

$$R_f=\frac{\Delta f_{d,measured}}{\Delta f_{d,predicted}} \quad (4)$$

where $\Delta f_{d,measured}$ is the measured value of the increased damping force after applying current and $\Delta f_{d,predicted}$ is the

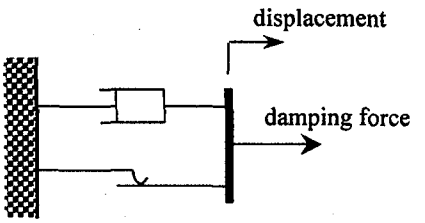

Fig. 5 The model of the MR damper

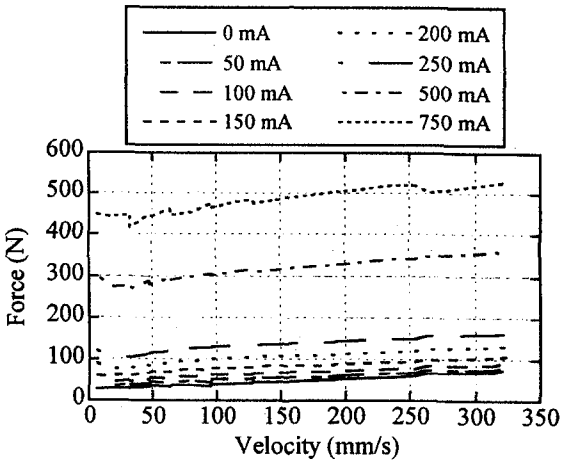

Fig. 6 Maximum force vs. velocity relationship

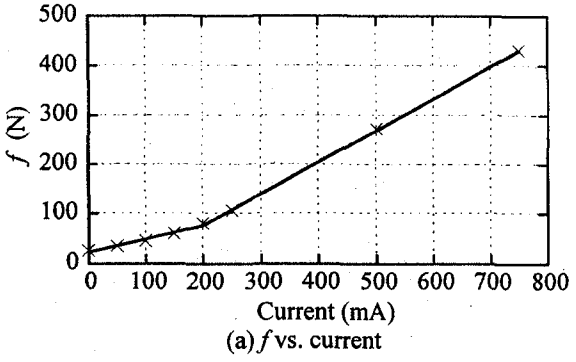

(a) f vs. current

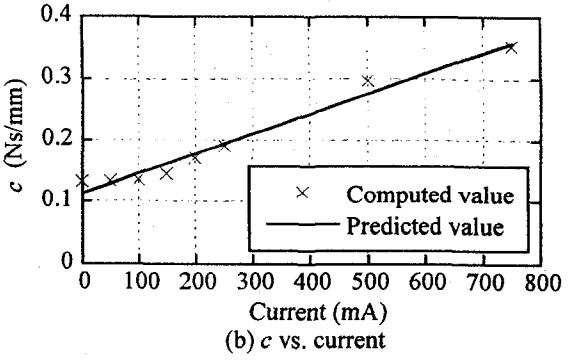

(b) c vs. current

Fig.7 The f and c values from the regression analysis

predicted value of the increased damping force after applying current. Fig. 11 shows the force ratio vs. time interval of applied current. It is seen that the force ratio approaches 1.0 when the time interval becomes longer than 140 ms. Consequently, it is considered that the rise time of this MR damper is 140 ms. Fig. 12 shows the increased damping force after applying current vs. fall time. The fall time increases with the increased damping force at the termination of current. The fall time is caused by the residual magnetic field in the MR damper. It is worthy to note that the rise time and fall time may limit the control of the damping force to some extent.

5. Control Algorithm and Experimental Verification

This study investigates two control algorithms that preset the damping force vs. displacement or velocity relationship. The purpose of the control algorithms is to dissipate energy and to break relative movement between two structures connected by the MR damper in order to prevent pounding or unseating.

Fig. 13 shows Algorithm 1 that damping force is commanded as a function of displacement[2]. When the absolute displacement is less than d_1, the damping force is set equal to f_1 that functions to dissipate energy. And when the absolute displacement exceeds d_1, the damping force is commanded to increase linearly to f_2 at d_2. The increase of damping force is intended to break the excessive relative movement.

Fig. 14 illustrates Algorithm 2 that the damping coefficient is varied with the displacement and velocity of the damper. When two structures are approaching or moving

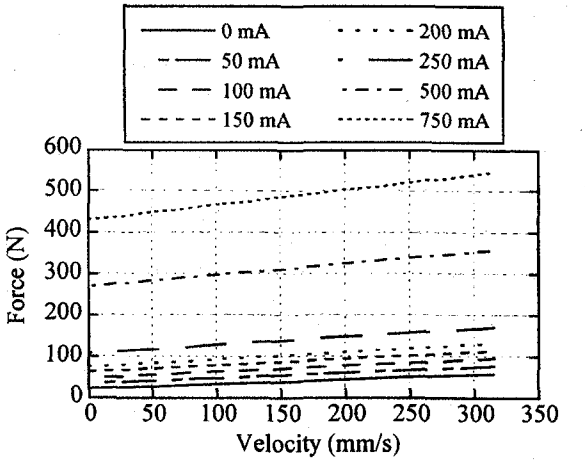

Fig. 8 Maximum force vs. velocity relationship by equations

apart from each other, the displacement and velocity have the same sign. In this case, the damping coefficient is set to a large value c_1. But when the displacement and velocity have the opposite sign, the damping coefficient is set to a small value c_2.

To study the extent to which the control algorithms can be implemented by the MR damper, a series of cyclic loading tests was performed. By applying the model of the MR damper, the control of damping force according to the control algorithm can be made. Algorithm 1 with d_1 = 10 mm, d_2 = 20 mm, f_1 = 80 N, and f_2 = 320 N was tested under the loading frequencies of 0.5, 1.0, 1.5, 2.0, 2.5, and 3.0 Hz and the loading amplitude of 20 mm. And Algorithm 2 with c_1=1.6 Ns/mm, and c_2=0.4 Ns/mm was tested under the same loading conditions.

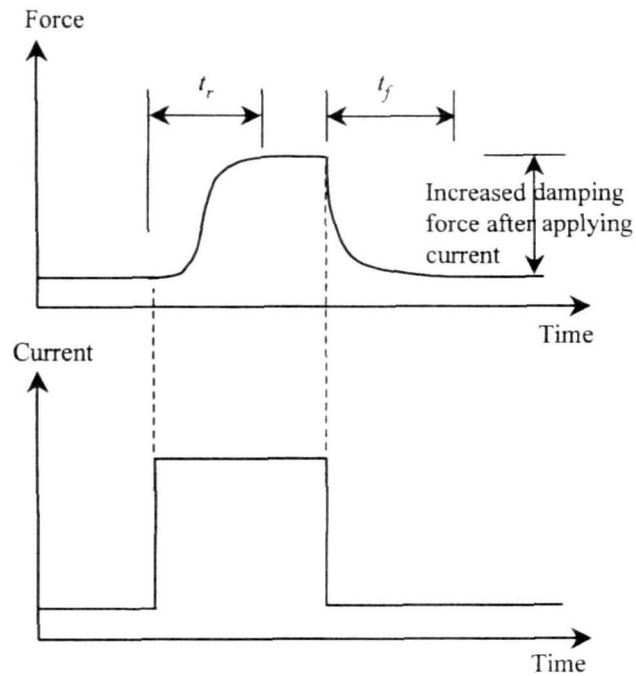

Fig. 9 Definition of the rise time and the fall time

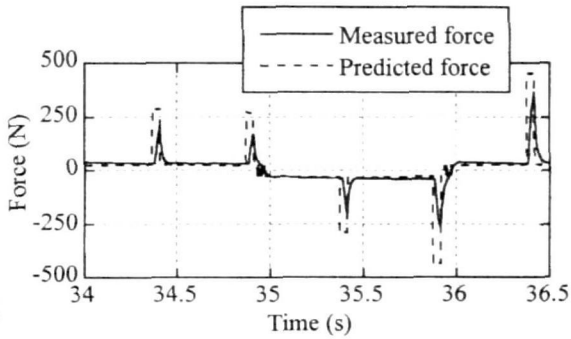

(a) time interval = 40 ms

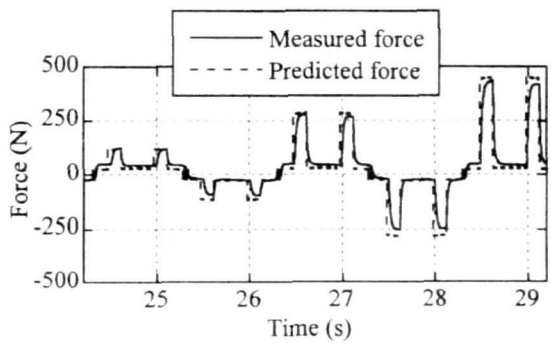

(b) time interval = 140 ms

Fig. 10 Comparison of predicted and measured damping force

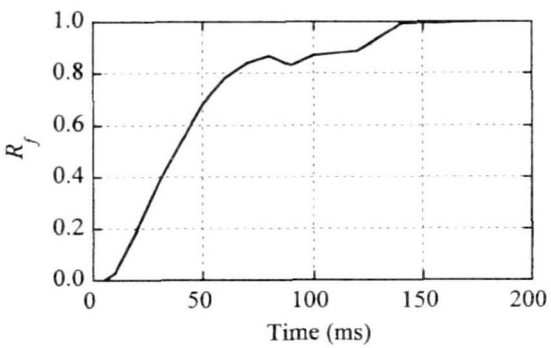

Fig. 11 R_f vs. time interval

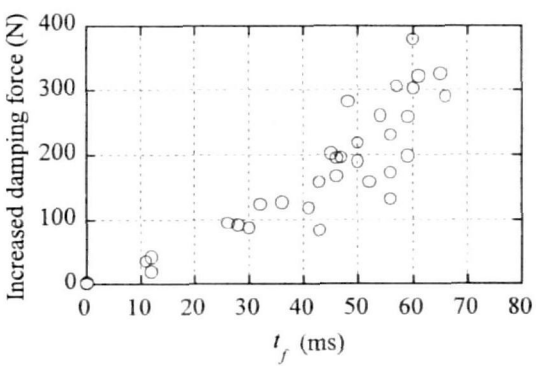

Fig. 12 Damping force vs. falling time

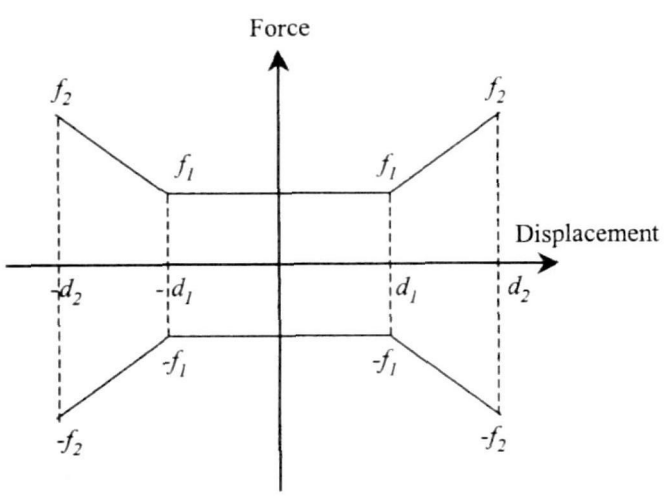

Fig. 13 Algorithm 1

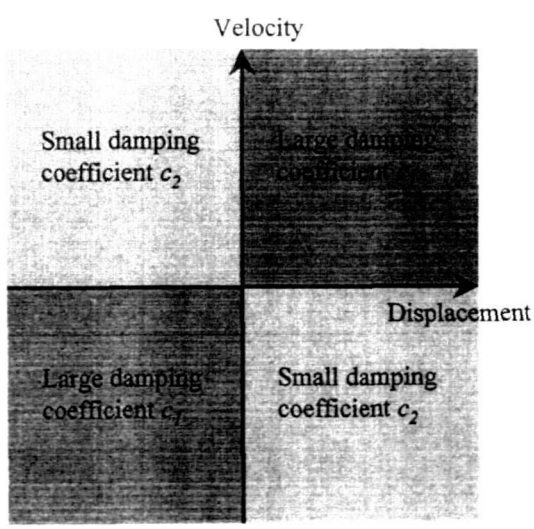

Fig. 14 Algorithm 2

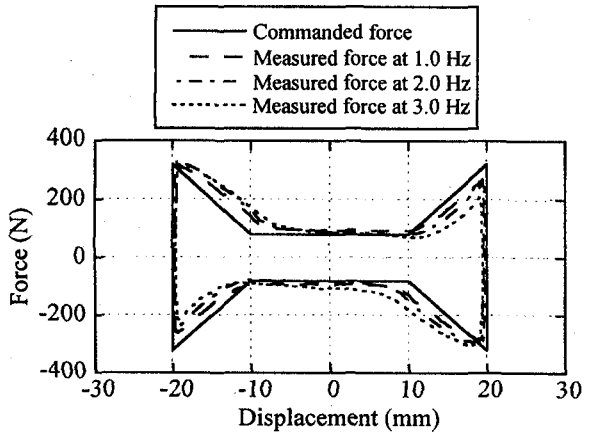

Fig. 15 Comparison of the measured and commanded force of Algorithm 1

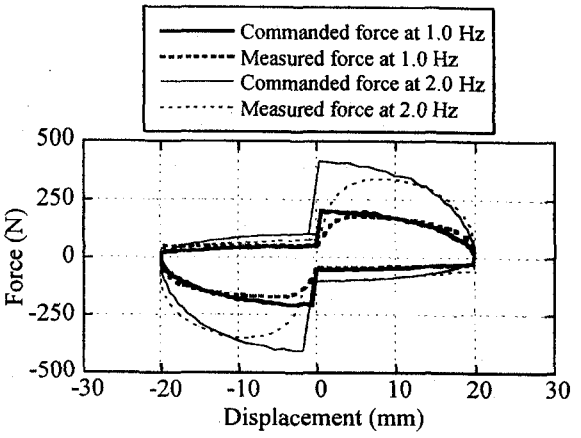

Fig. 16 Comparison of the measured and commanded force of Algorithm 2

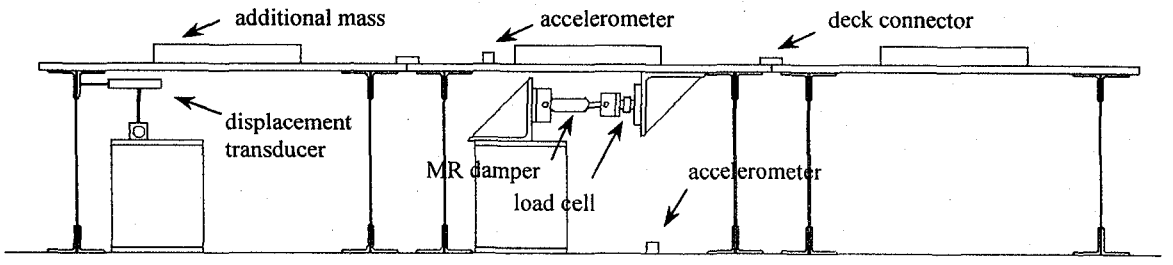

Fig. 17 Bridge model for shaking table test

Fig. 15 and Fig. 16 show the comparison between the measured and commanded force under various loading frequencies for Algorithms 1 and 2, respectively. It is found that the damping force can be produced according to the control algorithms. However, discrepancy of damping force is observed, especially when the rate of change of the damping force is high. As loading frequency increases, such discrepancy increases. The limited accuracy is resulted from the effect of the rise and fall time of the MR damper as mentioned above. Based on this experimental result, it is worthy to note that the sudden change of damping force as in Algorithm 2 may be difficult to realize in the control because it will cause impact in the damper and the structure. The smooth variation of the damping force is more realistic.

6. Shaking Table Test of Bridge Model with MR Damper

A shaking table test was performed on a bridge model with the MR damper. The bridge model used in the shaking table test and the measurement is illustrated in Fig. 17. The bridge model was composed of a three-span continuous deck and six piers. The MR damper was connected between the deck and the shaking table. The length of each span was 1.00 m and the height was 0.49 m. The mass of the deck was 370 kg. The deck and piers were made of steel plate and connected together by steel angles. Note that the same piers were used throughout the shaking table test. In some test cases, the piers experienced slight nonlinearity resulting from the stiffness deterioration. The progress of yielding was considered in the correlative study described later. A free vibration test of the bridge model without the MR damper was performed. It is found that the natural period is 0.58 s

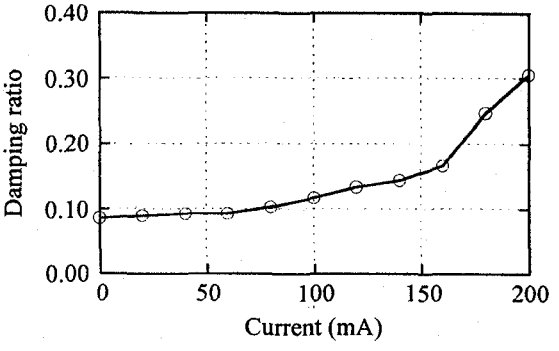

Fig. 18 Damping ratio vs. current

and the damping ratio is 1.2 %. The natural period of the bridge model is a typical value for a standard-size highway bridge. In addition, a free vibration test of the bridge model with the MR damper was performed for various current levels to the damper. Fig. 18 shows the variation of damping ratios with current levels. The damping ratio is about 8 % for zero current, and it increases to 30 % at the current level of 200 mA.

In the shaking table test, the bridge model was subjected to the NS component of the JMA Kobe record in the 1995 Hyogo-ken Nambu earthquake. Experimental cases of the shaking table test are listed in Table 1. Intensity of the ground acceleration was scaled down to 5% in the A-series test while it was 8% in the B-series test. The test was conducted in the sequence of A1, A2, A3, A4, A5, B2, B3, B5, B4, and B1.

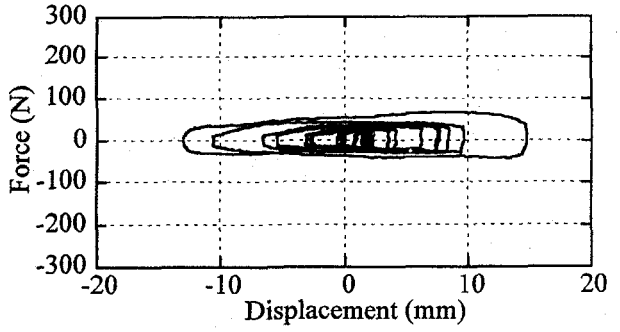

(a) case A1

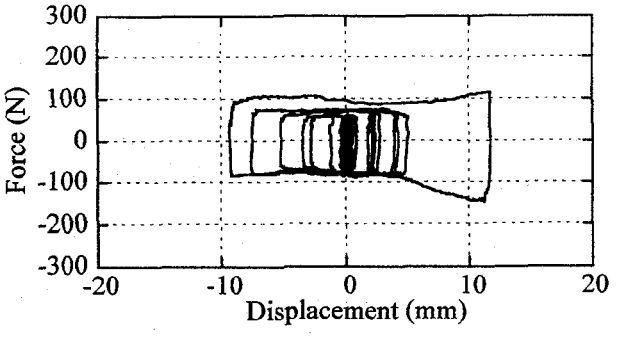

(b) case A2

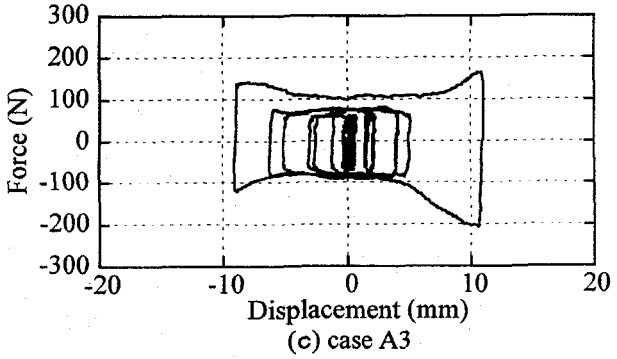

(c) case A3

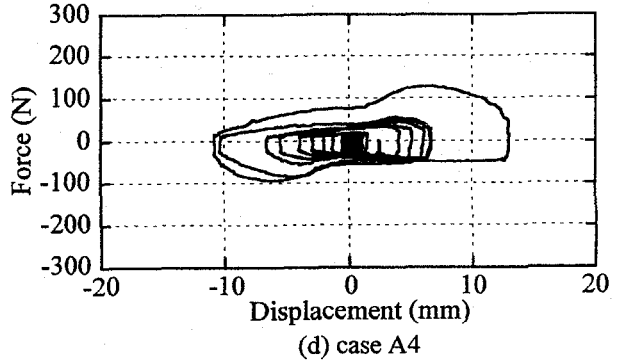

(d) case A4

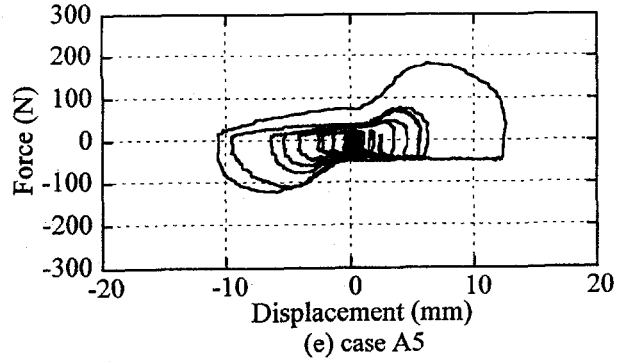

(e) case A5

Fig. 19 Damping force vs.displacement relationship for 5 % of JMA kobe record

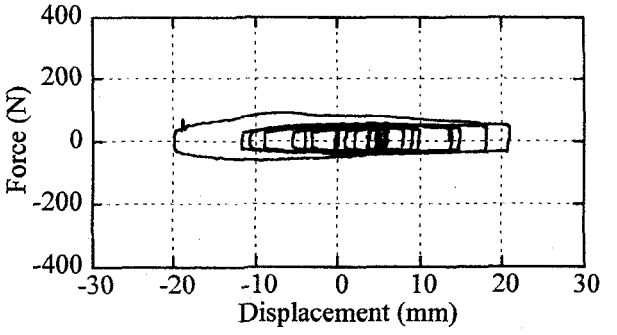

(a) case B1

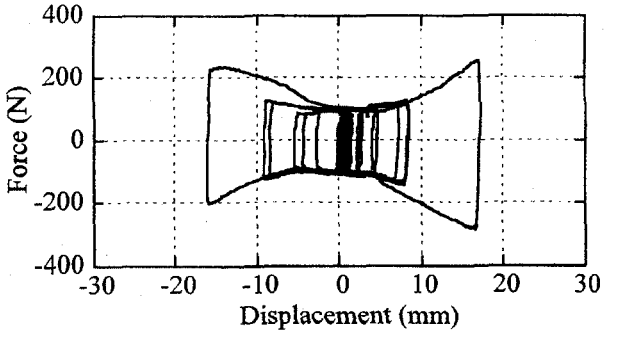

(b) case B2

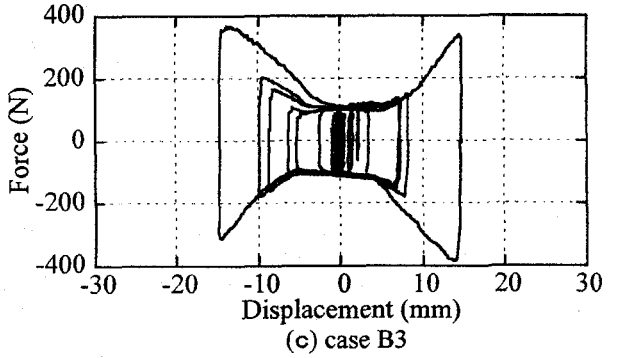

(c) case B3

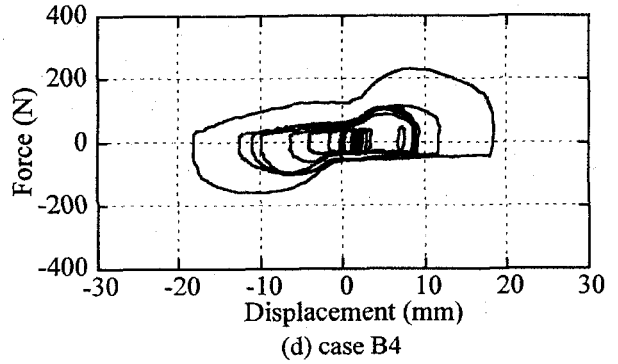

(d) case B4

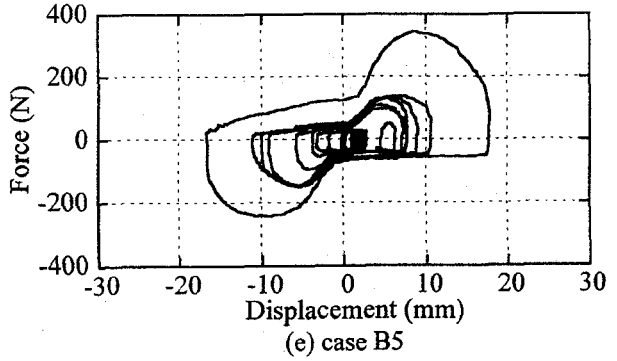

(e) case B5

Fig. 20 Damping force vs.displacement relationship for 8 % of JMA kobe record

Table 1 Experimental cases of the shaking table test

Case	Scale of Ground motion	Control Algorithm	Parameters
A1	5 %	-	current = 0 mA
A2	5 %	1	d_1 = 5 mm, d_2 = 10 mm f_1 = 80 N, f_2 = 160 N
A3	5 %	1	d_1 = 5 mm, d_2 = 10 mm f_1 = 80 N, f_2 = 240 N
A4	5 %	2	c_1 = 1.0 Ns/mm c_2 = 0.4 Ns/mm
A5	5 %	2	c_1 = 1.5 Ns/mm c_2 = 0.4 Ns/mm
B1	8 %	-	current = 0 mA
B2	8 %	1	d_1 = 5 mm, d_2 = 10 mm f_1 = 80 N, f_2 = 160 N
B3	8 %	1	d_1 = 5 mm, d_2 = 10 mm f_1 = 80 N, f_2 = 240 N
B4	8 %	2	c_1 = 1.0 Ns/mm c_2 = 0.4 Ns/mm
B5	8 %	2	c_1 = 1.5 Ns/mm c_2 = 0.4 Ns/mm

Table 2 Summary of experimental results from the shaking table test

(a) A-series test (5% of the JMA Kobe record)

control algorithm	variable	max. damping force (N)	max. dis-placement (mm)	residual dis-placement (mm)
Zero current	-	68	14.7	1.6
Algorithm 1 (d_1 = 5 mm, d_2 = 10 mm, f_1 = 80 N)	f_2 = 160 N	148	11.7	0
	f_2 = 240 N	207	11.0	0
Algorithm 2 (c_2 = 0.4 Ns/mm)	c_1 = 1.0 Ns/mm	129	13.0	0
	c_1 = 1.5 Ns/mm	183	12.5	0

(b) B-series test (8% of the JMA Kobe record)

control algorithm	variable	max. damping force (N)	max. dis-placement (mm)	residual dis-placement (mm)
Zero current	-	93	20.9	4.9
Algorithm 1 (d_1 = 5 mm, d_2 = 10 mm, f_1 = 80 N)	f_2 = 160 N	285	17.2	1.1
	f_2 = 240 N	385	14.9	0
Algorithm 2 (c_2 = 0.4 Ns/mm)	c_1 = 1.0 Ns/mm	233	18.4	1.3
	c_1 = 1.5 Ns/mm	344	17.7	1.2

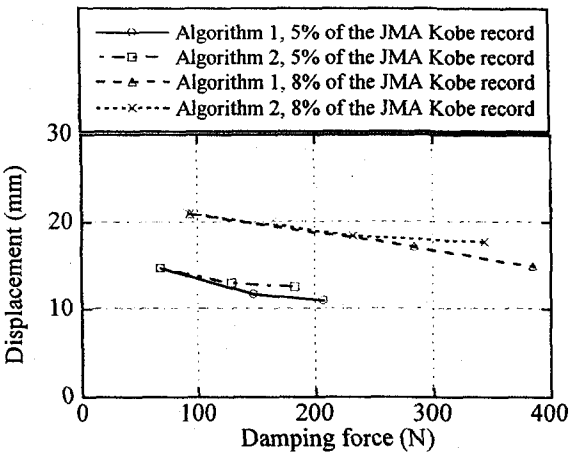

Fig. 21 Comparison of the control algorithms

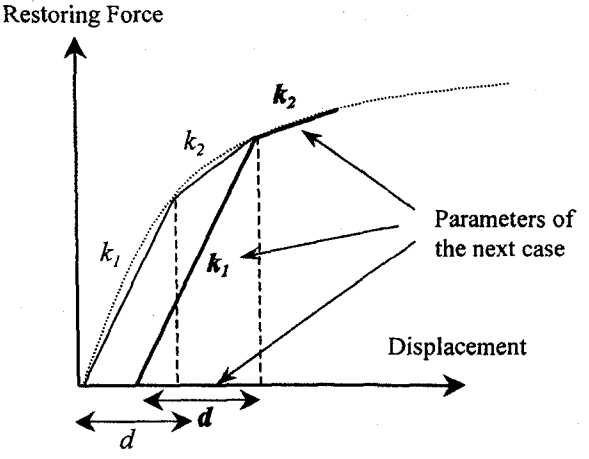

Fig. 22 Determination of parameters for the bilinear model

The force-displacement relationships of the MR damper of cases A1-A5 are illustrated in Fig. 19, and those of cases B1-B5 are illustrated in Fig. 20. The damping force can be realized according to the control algorithms with small discrepancy as explained. The experimental results for all cases are summarized in Table 2.

It is seen that when the current is zero in the A-series test, residual displacement of bridge response occurred after the excitation, resulting in the progress of the yielding of the piers. However, the residual displacement was very small in other cases of the A-series test. It is considered that the damping force provided by the MR damper was effective. Fig. 21 illustrates the maximum displacement vs. the maximum damping force. It is seen that as the damping force increases the displacement decreases. For both 5% and 8% of the JMA Kobe record, Algorithm 1 can reduce more displacement than Algorithm 2.

7. Correlative Study

The correlative study was performed to investigate the accuracy of the analysis in predicting the response of the bridge model with the MR damper. The bridge model is idealized as a single-degree-of-freedom system. The nonlinearity of bridge piers is represented as a bilinear model with the initial stiffness k_1, the second stiffness k_2 and the displacement d where the stiffness changes. It is important to note that the second stiffness defined here

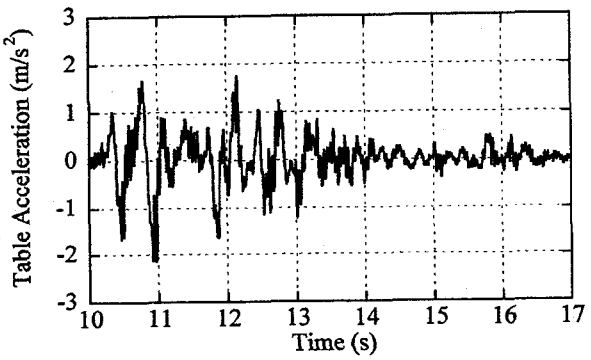

(a) Table acceleration

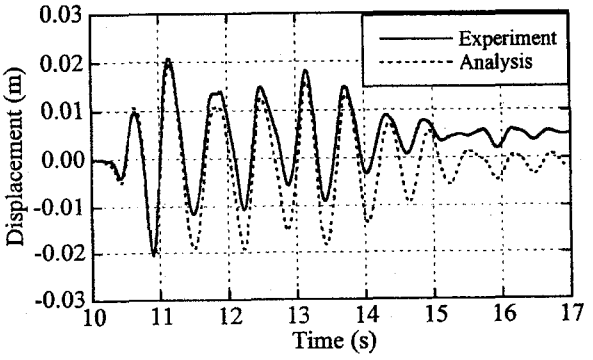

(b) Deck displacement

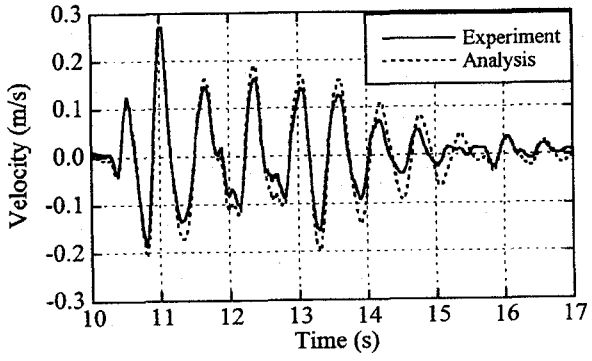

(c) Deck velocity

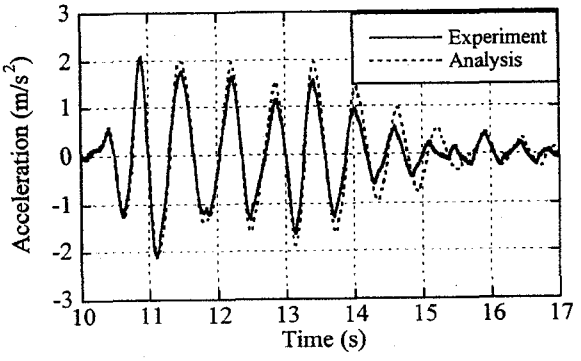

(d) Deck acceleration

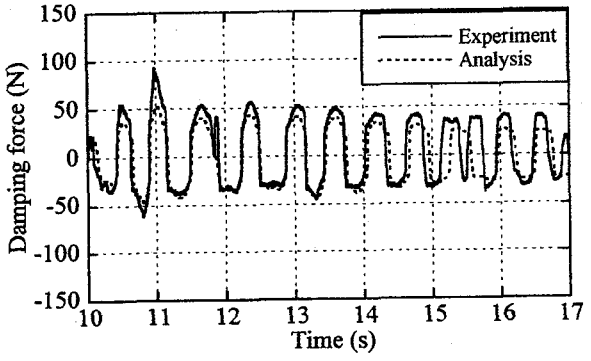

(e) Damping force

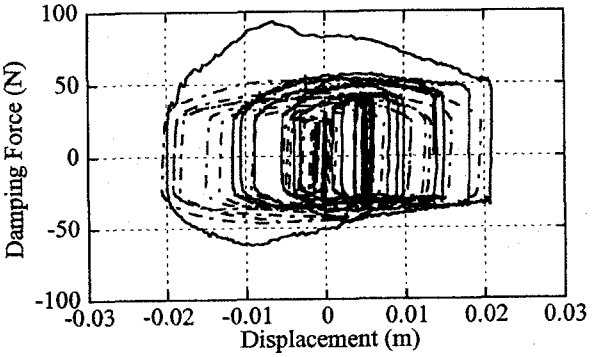

(f) Damping force vs. displacement relationship

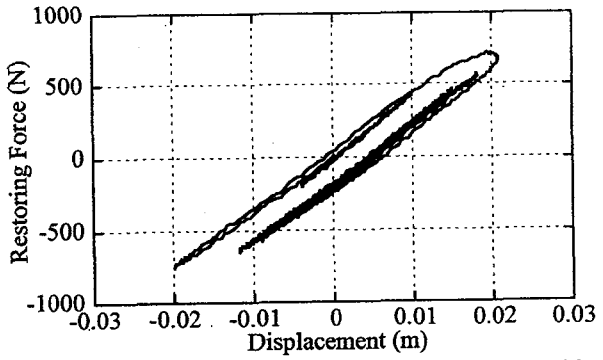

(g) Restoring force vs. displacement relationship of the piers

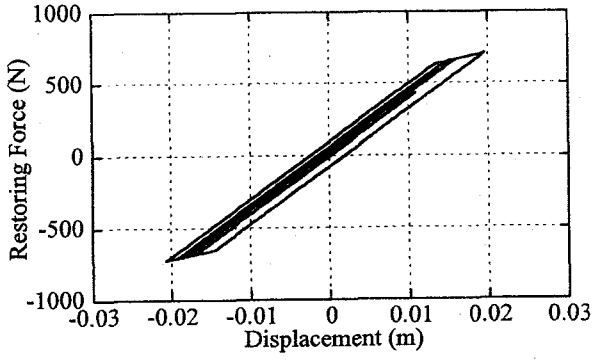

(h) Bilinear model of the piers

Fig. 23 Correlation for the response of the bridge model, with the MR damper under zero current, subjected to 8% of the JMA Kobe record (case B1)

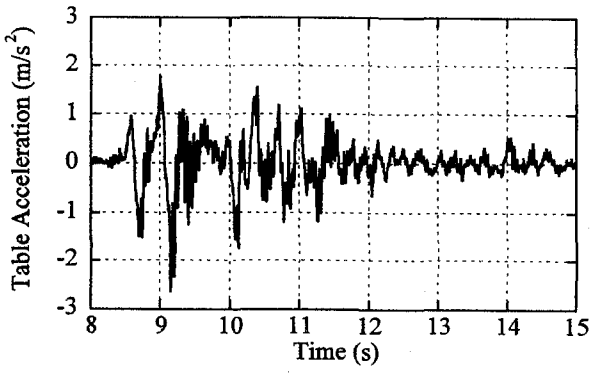

(a) Table acceleration

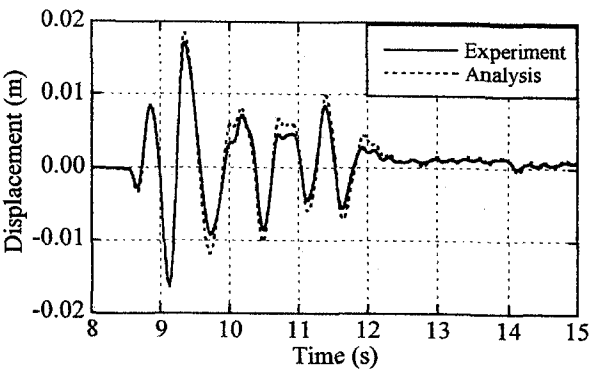

(b) Deck displacement

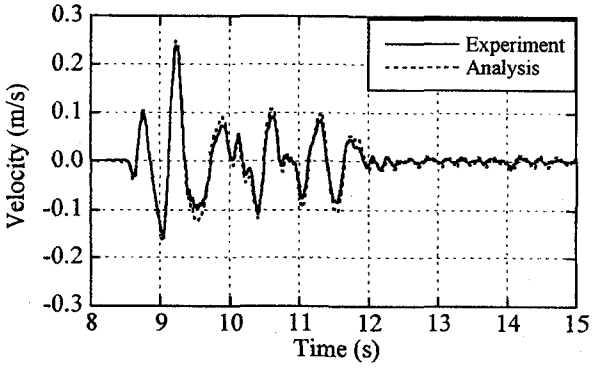

(c) Deck velocity

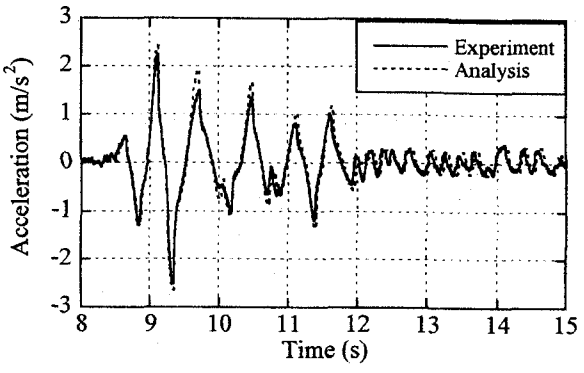

(d) Deck acceleration

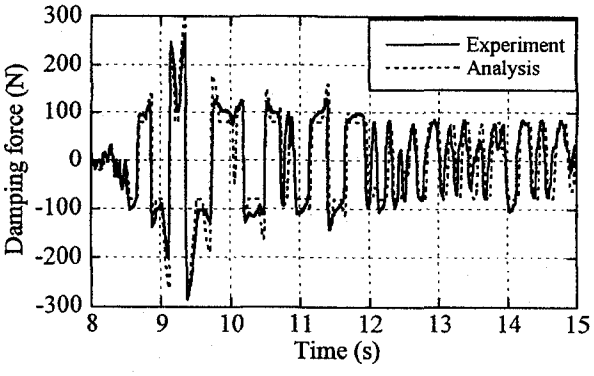

(e) Damping force

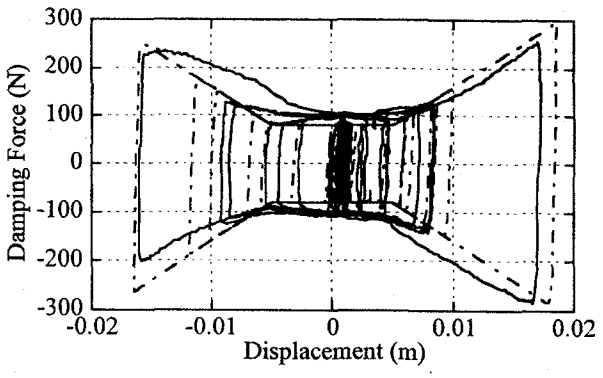

(f) Damping force vs. displacement relationship

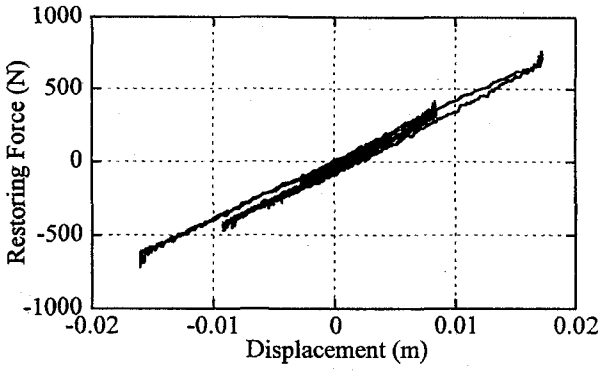

(g) Restoring force vs. displacement relationship of the piers

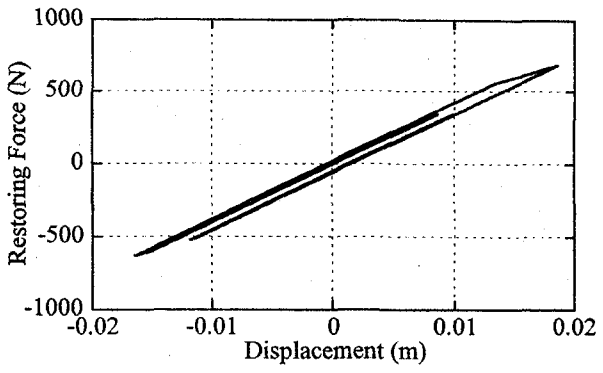

(h) Bilinear model of the piers

Fig. 24 Correlation for the response of the bridge model, with the MR damper controlled by Algorithm 1, subjected to 8% of the JMA Kobe record (case B2)

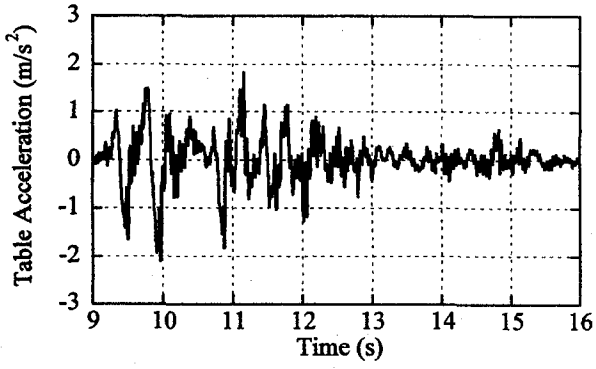

(a) Table acceleration

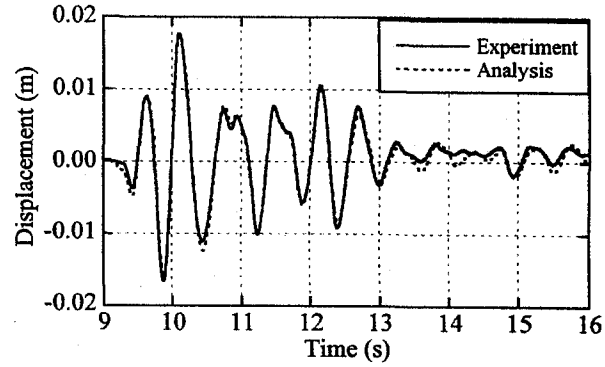

(b) Deck displacement

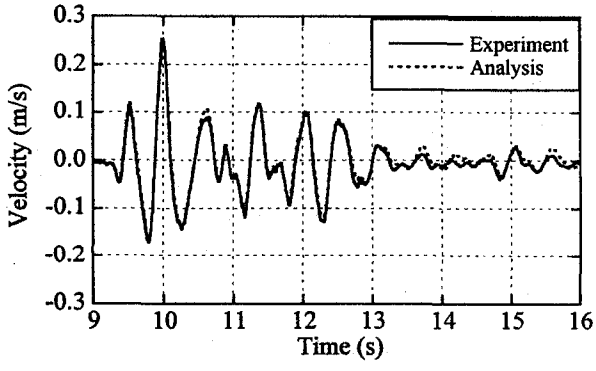

(c) Deck velocity

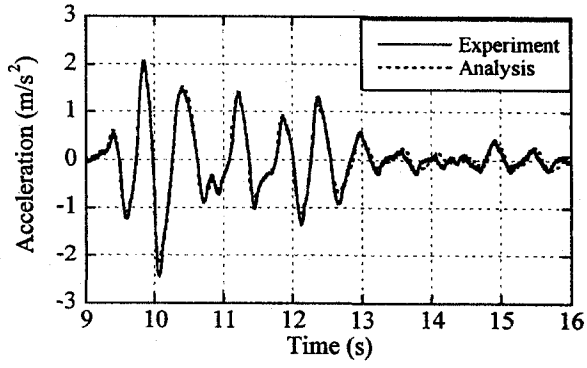

(d) Deck acceleration

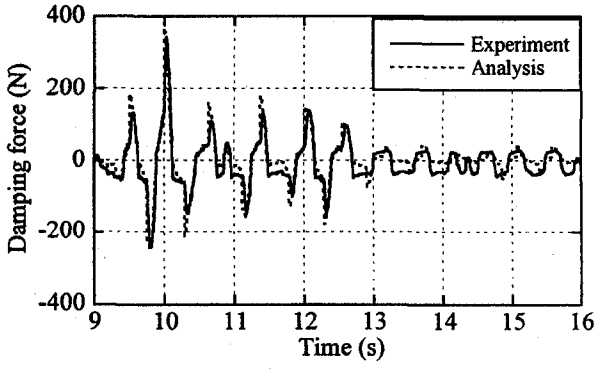

(e) Damping force

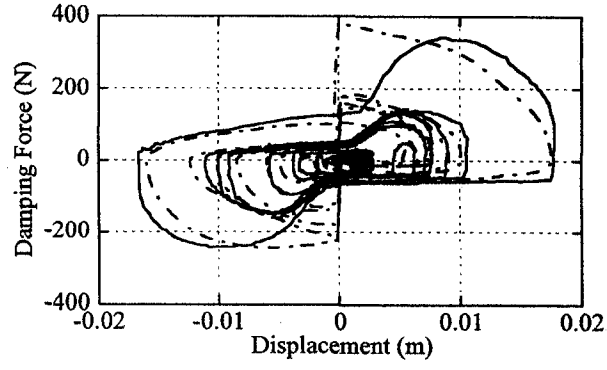

(f) Damping force vs. displacement relationship

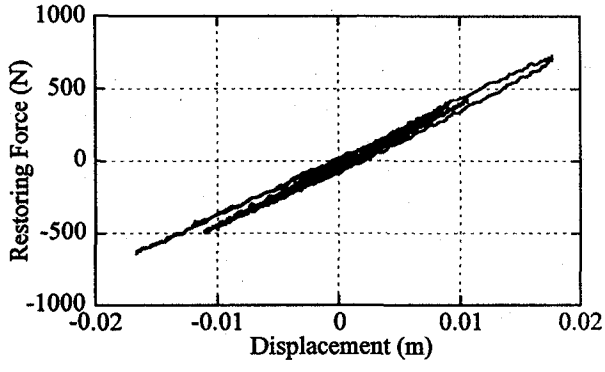

(g) Restoring force vs. displacement relationship of the piers

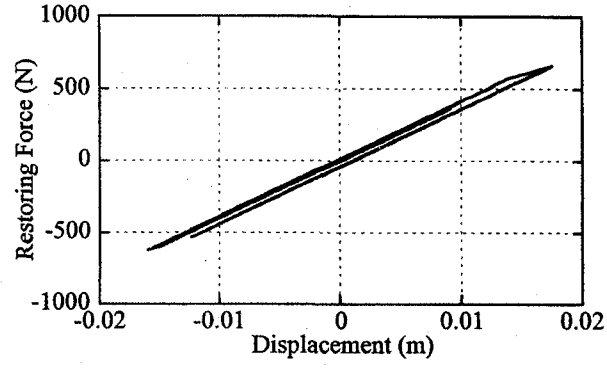

(h) Bilinear model of the piers

Fig. 25 Correlation for the response of the bridge model, with the MR damper controlled by Algorithm 2, subjected to 8% of the JMA Kobe record (case B5)

Table 3 The k_1, k_2, and d values used in the correlative analysis

Sequence	Case	k_1 (N/m)	k_2 (N/m)	d (m)
1	A1	43000	25800	0.013
2	A2	43000	25800	0.013
3	A3	43000	25800	0.013
4	A4	43000	25800	0.013
5	A5	43000	25800	0.013
6	B2	40000	24000	0.015
7	B3	40000	24000	0.015
8	B5	40000	24000	0.015
9	B4	40000	12000	0.017
10	B1	40000	12000	0.017

represents the stiffness in the yield-transient zone, and it is larger than the post-yielding stiffness. The restoring force of the piers f_s is evaluated from

$$f_S = -\left(ma+c\dot{u}+f_d\right) \tag{5}$$

where m is the mass of the deck, c is the damping coefficient, a is the measured absolute acceleration of the deck, u is the measured deck displacement relative to the shaking table, and f_d is the measured damping force of the MR damper. The parameters for the bilinear model are determined from the computed restoring force vs. displacement hysteresis of the piers. Because the same piers were used throughout the shaking table test, the yielding of the piers gradually progressed. Hence, it is required to modify the k_1, k_2, and d values as shown in Fig. 22 to obtain the best correlation. Table 3 shows the k_1, k_2, and d values thus used in the analysis. They are presented in the sequence of the test. It should be note that as the yielding of the piers progresses, k_1 and k_2, decrease while and d increases in a monotonic manner.

Fig. 23 illustrates the correlation for the response of the bridge model, with the MR damper under zero current, subjected to 8% of the JMA Kobe record (case B1). It is seen that the computed responses represent the overall behavior of the bridge model in the shaking table test. Only some discrepancy arises in the deck displacement. The experimental deck displacement has some drift after 11.5 s and exhibits slightly biased response in the positive direction, while the analytical deck displacement does not have such drift and is almost symmetric around the rest position. It is seen from Figs. 23 (e) and (f) that the experimental damping force is about 1.6 times of the analytical damping force. This resulted in the discrepancy of the deck displacement. It is required to make more investigation on the characteristics of the MR damper at zero current under random excitation.

Fig. 24 illustrates the correlation for the response of the bridge model, with the MR damper controlled by Algorithm 1, subjected to about 8% of the JMA Kobe record (case B2). Good agreement between the experimental and analytical results is obtained. It is seen in Fig. 24 (f) that the analytical damping force at its extreme values is quite close to the experimental damping force.

Fig. 25 illustrates the correlation for case B5. It is seen that the good agreement between the experimental and analytical results is obtained as seen from the time histories of the bridge response.

8. Conclusions

The study on the application of a MR damper for semi-active control of bridges is conducted by a series of cyclic loading tests and shaking table tests. From the investigation presented herein, it may be concluded as

1) From the results of cyclic loading test of the MR damper under various loading conditions and current levels, it is found that damping force depends on input current levels and velocity. The MR damper can be idealized with good accuracy by the model of friction and viscous elements in parallel.

2) In actual application, the MR damper is subjected to fluctuating current. The accuracy of the model is limited by the time required for MR fluid to reach its rheological equilibrium. The rise time is 140 ms for the damper used in this study. The fall time increases with the increased force after applying current.

3) The damping force is commanded according to two control algorithms that vary damping force with displacement or velocity. It is found that damping force can be generated according to the control algorithms. However, discrepancy is observed, especially when the rate of change of the damping force is high and the loading frequency increases.

4) From the shaking table test, it is found that Algorithm 1 provides slightly more reduction of displacement than Algorithm 2 at the same amount of damping force.

5) Correlative study was conducted on a bridge model with a MR damper. It is found that the response of the bridge model with the MR damper under the control algorithms can be represented by the analysis with good accuracy.

Acknowledgements

The magnetorheological damper used in this study is provided by Sanwa Tekki Corporation. The authors appreciate Dr. Katsuaki Sunakoda and Mr. Hiroshi Sodeyama for their kind cooperation. The authors are thankful to Professor Billie F. Spencer, University of Notre Dame for his comments. Special thanks are due to Mr. Gaku Shoji, Mr. Gakuho Watanabe, and Mr. Kenji Uehara for their contributions in conducting the cyclic loading test and shaking table test.

References

1) Symans, M. D. and Constantinou, M. C., Semi-Active Control Systems for Seismic Protection of Structures: a State-of-the-Art Review, *Engineering Structures*, 21, pp. 469-487, 1999.

2) Kawashima, K. and Unjoh, S., Seismic Response Control of Bridges by Variable Dampers, *Journal of Structural Engineering, ASCE*, 120-9, pp. 2583-2601, 1994.

3) Spencer, B. F., Dyke, S. J., Sain, M. K., and Carlson, J. D., Phenomenological Model of a Magnetorheological Damper, *Journal of Engineering Mechanics, ASCE*, 123-3, pp. 230-238, 1997.

4) Sunakoda, K., Sodeyama, H., Iwata, N., Fujitani, H., and Soda, S., Dynamic Characteristics of Magneto-Rheological Fluid Damper, *SPIE 7th Annual Int. Symposium on Smart Structures and Materials*, Newport Beach, USA, 2000.

(Received September 14, 2000)